## PAPER

Check for updates

# Combinatorial ALD for the growth of ZnO/TiO$_2$ nanolaminates and mixed ZnO/TiO$_2$ nanostructured films

Shóna Doyle, [ID] *[a] Louise Ryan,[a] Melissa M. McCarthy, [ID] [ab] Mircea Modreanu,[a] Michael Schmidt,[a] Fathima Laffir,[c] Ian M. Povey [ID] [a] and Martyn E. Pemble [ID] [ad]

In this study, combinatorial atomic layer deposition (C-ALD) has been used to deposit layered ZnO and TiO$_2$ nanolaminates on both oxide-covered Si(100) wafers and glass substrates to assess the influence of substrate and each layer on the structure of the resulting nanolaminates and their photoactivity towards dye degradation. In addition, for comparison to these layered structures, C-ALD has been used to directly create oxide films consisting of an approximately equal mixture of Zn$^{2+}$ and Ti$^{4+}$ ions using the concept of under-dosing in order to deposit sub-monolayer quantities of each oxide per complete C-ALD cycle. A nucleation delay was observed for ZnO deposited directly on the substrate and the subsequent TiO$_2$ layer, the latter to a lesser extent. The reason for the difference in nucleation delay is due to the dissimilar surface groups. For the deliberately layered structures, it was found that ZnO appeared to possess a templating influence on the TiO$_2$ layer grown subsequently on both substrate types. XRD analysis showed strong preferential orientation for (002) which indicates the polycrystalline manner of the ZnO film. XRD results also suggested that layer growth was substrate-dependent as crystalline TiO$_2$ was only identified on glass substrates. The nanolaminate structures were found to be stable in that the layer structure remained intact after annealing at 400 °C for 1 hour in contrast to the comparison to the mixed ZnO : TiO$_2$ (1 : 1) film which showed evidence of ZnO segregation and crystallisation. Concerning photocatalytic activity, no evidence was found for any enhancement of photoactivity in the mixed or nanolaminate films, the most photoactive films being those consisting of ZnO deposited onto glass substrates.

## Introduction

Thin film materials are an essential part of the modern world being relevant to all aspects of society as may be easily appreciated when one considers electronics, energy, communications and medical issues. Nanostructured materials offer unique, but more often unknown potential benefits that could positively be applied in all of the areas cited arising from the fact that the properties of atoms, groups of atoms and ultra-thin layers are exploited rather than bulk materials.

Hybrid nanolaminate materials have attracted great attention in recent years due to the physical and chemical properties that 2D nanosheets possess that their bulk counterparts do not

such as electrical,[1,2] mechanical,[3] optical[4–6] and thermal properties.[7] The number of publications on the topic is increasing and is predicted to continue to increase.[8] Noteworthy reviews exist on the topic which explore the fundamentals and importance of these materials[8–10] and also with a focus on specific application fields.[11] The applications of hybrid films are almost endless, ranging from use as capacitors,[12–15] dielectrics and insulators,[16–25] encapsulation layers/protective coatings,[26–34] lubricants[35] and optical waveguides.[36]

Specifically, nanolaminates are multicomponent systems consisting of alternating layers of materials such as metals and metal oxides. Each layer has an associated thickness on the nanometre scale.[37] Mixing a wide variety of materials makes it possible to fine-tune a material in terms of its properties, composition and structure.[38] Films of this type can be readily prepared using atomic layer deposition (ALD) – particularly when deployed in a combinatorial sense using multiple precursors, since ALD is a method that is capable of producing precise films with constant thickness.[39,40] A similar approach has been used in various CVD processes where the term

$^a$ *Tyndall National Institute, University College Cork, Cork, Ireland.*
 *E-mail: shona.doyle@tyndall.ie*

$^b$ *Department of Physics, University of Oxford, Clarendon Laboratory, Parks Road, Oxford, UK*

$^c$ *Department of Chemical Sciences and Bernal Institute, University of Limerick, Limerick, Ireland*

$^d$ *School of Chemistry, University College Cork, Cork, Ireland*

combinatorial CVD has been employed.[41–45] By analogy, we name our process combinatorial ALD or C-ALD in order to describe a process in which the individual ALD processes for the growth of two or more materials are combined. The use of the term C-ALD simply gives these mixed ALD processes a collective name and distinguishes them from processes that involve only one type of material growth cycle. The unique conformity and precision of ALD enables sub-nanometre design and control of these true nanolaminates thus facilitating the realisation of unique materials properties through this combinatorial approach. Indeed C-ALD provides a route to the fabrication of a truly vast number of potentially new materials, being based on sets of layers of differing materials, layers consisting of mixtures of sub-monolayer quantities of various materials, materials where doping is spread or confined to particular layers or even the creation of new types of alloys.

Using C-ALD it is thus potentially possible to create materials that have new electronic, magnetic and optical properties. Many such properties depend on bulk phenomena which then manifest as new surface phenomena.[41] Photocatalytic activity is a good example of such a phenomenon, in which the creation of excitons *via* the absorption of light of energy greater than the band gap of the material results in the formation of highly oxidizing surface species, capable of destroying organic materials such as pollutants and micro-organisms. Arguably, the most well-known examples of photocatalytically active metal oxide materials are $TiO_2$ and ZnO.

Both ZnO and $TiO_2$ are wide band gap semiconductors with band gap energies in the region of 3.2–3.4 eV.[42,43] The similarity in band gap energies of $TiO_2$ and ZnO and their similar photocatalytic mechanisms suggest $TiO_2$ and ZnO as suitable materials to be coupled together. Previous work synthesizing $ZnO/TiO_2$ laminates involved the use of E-beam evaporation,[44] sol–gel methods,[44–46] ALD[47–49] and spatial ALD[50] with alternative precursors. The findings of these studies showed improvements in crystallinity and quality of ZnO as a direct consequence of a $TiO_2$ under layer,[44] the successful degradation of organic dyes,[45,46] enhanced friction coefficients[49] and increased GPC of $TiO_2$ when deposited on ZnO as opposed to itself.[48] Interestingly, as the number of bilayers increased with the total thickness and composition of the films remaining the same, an enhancement of the optical transmittance was observed.[47,50] XRD spectra of nanolaminates revealed weaker signature peaks for the same thickness nanolaminates with more bilayers, suggesting the possibility of tuning nanolaminates from crystalline to amorphous phase. As the number of bilayers decreased for films with the same overall thickness, the refractive index (RI) decreased.[50]

In terms of the photocatalytic properties of both ZnO and $TiO_2$ it is interesting to consider whether the functionalities will both act together and be enhanced or degraded when the materials are combined in various nanolaminate structures. Possible enhancements of photocatalytic activity may arise from greater photocarrier separation arising for example from the ability of ZnO to act as an electron transport layer.[51–54] On the other hand a loss in photocatalytic activity may arise from structural factors related to templating effects.

In order to try to examine these and other potential issues we have studied the growth of nanolaminates of ZnO and $TiO_2$ using a C-ALD approach. Nanolaminate structures have been prepared with the specific aim of combining the photocatalytic properties and robustness of $TiO_2$ with the transparent conducting behaviour and photoactivity of ZnO. In addition we have grown a mixed $ZnO/TiO_2$ layer by deliberately underdosing during the metal precursor parts of the ALD cycle. Fig. 1 and 2 are schematic representations of the structures grown and examined here. The spacing and thickness of the ZnO and $TiO_2$ layers in the nanolaminates have been carefully controlled and the resulting materials studied using electron microscopy, atomic force microscopy and optical absorption spectroscopy. In addition the photocatalytic properties of the layers were examined using a combination of contact angle measurements and a simple dye test, comparing $TiO_2$ layers both with and without ZnO under-layers (and *vice versa*), in order to assess the magnitude and range of ZnO templating influence on the photo active nature of the $TiO_2$.

## Experimental

### Preparation of $TiO_2/ZnO$ composites

$TiO_2/ZnO$ bilayer laminate films were deposited on glass and Si(100) substrates using a Cambridge Nanotech Fiji 200 ALD system. Diethyl zinc (DEZn) (min. 95% Strem Chemicals), tetrakis(dimethylamido)titanium(IV) (TDMAT) (99% Strem Chemicals) and water were used as precursors at a growth temperature of 200 °C. Argon (Ar) was used a carrier gas to transport the precursor molecules into the chamber. During the deposition process, the diethyl zinc and water were sustained at room temperature while the temperature of the titanium precursor container; was set to a temperature of 80 °C to ensure sufficient vapour pressure was generated. Pulse times were 0.4 s, 0.2 s and 0.1 s for TDMAT, diethyl zinc and water respectively accompanied with a 10 s argon purge between precursor pulses to remove redundant ligands. The deposition rate was controlled at 2 Å per cycle for ZnO layers and 0.5 Å per cycle for $TiO_2$ layers. The deposition depth of both ZnO and $TiO_2$ layers was 40 nm. Films were produced with ZnO layer (40 nm) followed by $TiO_2$ layer (40 nm) and *vice versa*. For comparison, $TiO_2$ and ZnO films were grown with a thickness of 40 nm using the same precursors already mentioned. A laminate consisting of ZnO and $TiO_2$ multilayers, (4 nm ZnO + 4 nm $TiO_2$) ×5 was grown. A deliberately mixed $ZnO/TiO_2$ 1:1 film was also grown by alternating very short (0.05 s)
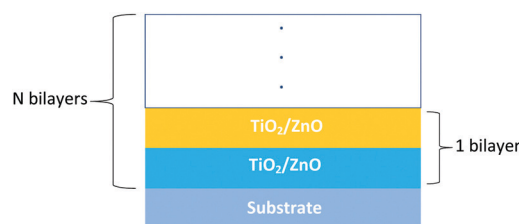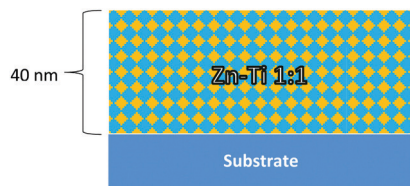


Fig. 1 Schematic of the $TiO_2/ZnO$ nanolaminates.

**Fig. 2** Schematic of the true $ZnO:TiO_2$ 1 : 1 nanolaminate.

pulses of each precursor until the desired thickness of 40 nm was reached.

### Characterization techniques

The surface morphology of the film was observed using scanning electron microscopy (SEM) using a FEI Quanta 650 FEG High Resolution Scanning Electron Microscope. The crystallinity of the $TiO_2/ZnO$ films was analysed by X-ray diffraction (XRD) using a PANalytical X'Pert Pro diffractometer, with Cu Kα ($\lambda$ = 0.154 nm) radiation from 10 to 70° at a step size of 0.02° under 45 kV and 30 mA. Grazing incidence XRD (GIXRD) was carried out on a Rigaku Ultima with an incidence angle of 2°. The XRD results were compared to the Joint Committee on the Powder Diffraction Standard cards (JPCDS). The interface of the bilayer was observed using transmission electron microscopy using FIB/TEM (JEOL JEM 2100). Atomic Force Microscopy (AFM) measurements were carried out in the non-contact mode, with an XE-100 apparatus from Park Systems, using sharp tips. The topographical 3D AFM images were taken over the area of $1 \times 1$ $\mu m^2$. The images were processed with XEI (v.1.8.0) Image Processing Program developed by Park Systems. The UV-Vis transmission spectra were recorded in the range of 200–1000 nm using a PerkinElmer Lambda 950 UV/VIS/NIR spectrometer. The composition and binding energies of the films were investigated by X-ray photoelectron spectroscopy (XPS) using a Kratos AXIS_ULTRA spectrometer with the following parameters; sample temperature: 20–30 °C and X-ray gun: mono Al Kα 1486.58 eV; 150 W (10 mA, 15 kV). Samples were sputtered with Argon Gas Cluster source (10 keV, Ar1000+ clusters) for 2–3 s in order to remove the carbon over layer contact angle (CA) measurements were obtained using a Data Physics OCA 15EC system utilising a sessile drop arrangement at room temperature. A Hamilton 100 μL syringe was used to dispense 1 μL water droplets onto the surface. Small volumes were beneficial to avoid gravity-induced drop shape alteration and to diminish evaporation effects during CA measurements.

### Evaluation of photocatalytic activity

The photocatalytic activity was evaluated by degradation of dye under UV light irradiation. A dropper was used to add the dye of choice to the top of the film and a metal rod (3 mm K-bar) was used to spread the dye across the film. The dye was allowed to dry and subsequently exposed to UV light (3.30 mV cm$^{-2}$). A qualitative approach was applied to monitor and record the dye degradation over time which involved the use of a handheld digital scanner.

## Results and discussion

### The surface morphologies and structural properties of $TiO_2/ZnO$ films

Fig. 3 shows the GIXRD pattern of selected samples. For both ZnO grown on $TiO_2$ and *vice versa*, the most predominate peaks can be attributed to hexagonal ZnO with the (002) peak being most evident. Strong preferential orientation for (002) indicates the polycrystalline manner of the ZnO film. This corresponds to wurtzite ZnO. On glass substrates, peaks are again visible for hexagonal ZnO but interestingly also seen are peaks that may be attributed to anatase $TiO_2$. The GIXRD patterns suggest that ZnO is somewhat crystalline. Interestingly, the XRD pattern of both $ZnO:TiO_2$ (1 : 1) and $ZnO–TiO_2$ (bilayer ×5) appear to be strikingly similar on both glass and Si(100) substrates. A crystalline peak at approximately 52° on the Si(100) substrate is seen for both films and is assigned to $TiO_2$(105), indicative of the anatase phase. The observed GIXRD peaks compare to standard JCPDS file data.

SEM reveals that the underlying structure of the ZnO layer affects the structure of the $TiO_2$ grown on top. This can be seen by comparing the morphology of $TiO_2$ grown directly on the substrate *versus* $TiO_2$ grown on ZnO (Fig. 4 and 5). The morphology is comparable to ZnO. Growth also appears to be substrate-dependent based on the SEM images obtained. A difference can be seen between $TiO_2$ deposited on (a), the oxide-covered Si(100) substrates and (b), the glass substrates.
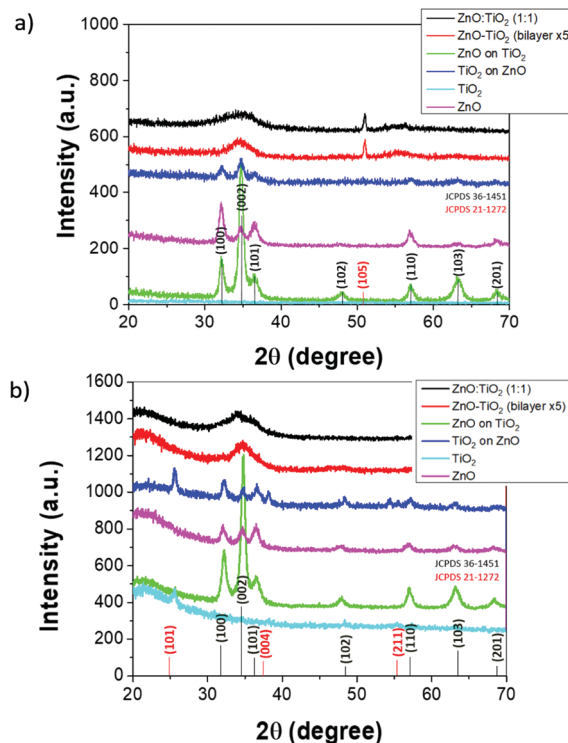


**Fig. 3** GIXRD patterns recorded from $TiO_2$ (light blue), ZnO (pink), $TiO_2$ on ZnO (dark blue) and ZnO on $TiO_2$ (green), $ZnO–TiO_2$ ×5 bilayer (red) and $ZnO:TiO_2$ 1 : 1 (black) grown on (a), an oxide-covered Si(100) substrate and (b), glass substrates. See insert caption for detail.
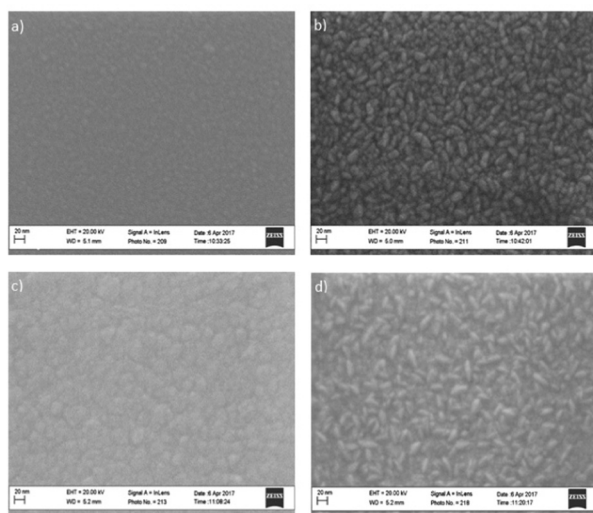
**Fig. 4** SEM images following ALD growth on Si(100) substrates: (a) TiO$_2$ (b) ZnO (c) TiO$_2$ on ZnO and (d) ZnO on TiO$_2$.
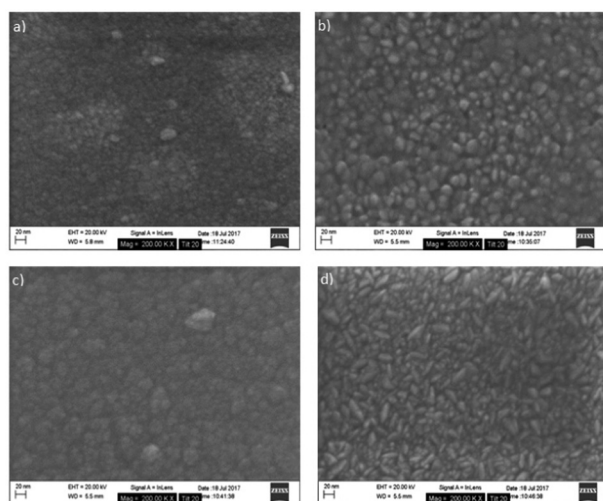


**Fig. 5** SEM images following ALD growth glass substrates: (a) TiO$_2$ (b) ZnO (c) TiO$_2$ on ZnO and (d) ZnO on TiO$_2$.

Larger surface features are evident on the glass substrate. These data are analysed further in a later section.

The Scherrer eqn (1) was applied which relates the full width at half maximum height (FWHM) for the XRD peaks to the grain size.

$$D = \frac{K\lambda}{\beta \cos \theta} \quad (1)$$

where $K$ is the shape factor, $\lambda$ is the X-ray wavelength, $\beta$ is the FWHM (full width at half maximum) (radians) and $\theta$ is the angle of diffraction. The FWHM for the ZnO(002) peak was used in the equation. A comparison was made with grain sizes obtained *via* the Scherrer method[55] and the intercept method.[56] The results are seen below in Table 1. Grain sizes obtained by the Scherrer method were consistently smaller

**Table 1** Comparison of crystallite size calculated by the Scherrer equation and the intercept method along to ZnO(002) crystal plane

| Thin film | | Scherrer method crystallite size (nm) | Intercept method crystallite size (nm) |
|---|---|---|---|
| ZnO on TiO$_2$ | Si | 12.1 | 22.7 |
| | Glass | 12.0 | 21.9 |
| TiO$_2$ on ZnO | Si | 14.9 | 29.3 |
| | Glass | 15.0 | 29.5 |

than those obtained using the intercept method. For the latter, measurements correspond to random but forced fixed placement of a line on an image. Therefore, observer interpretation and variations in patterns must be considered. In the case of ZnO, rod-like grains have random placement which does not lend itself to accurate measurement *via* the intercept method.

Transmission electron microscopy (TEM) images are presented in Fig. 6. In these images the darker layer is ZnO and the lighter layer is TiO$_2$. The brighter layer seen below the TiO$_2$ is a SiO$_2$ interfacial layer as the Si(100) substrate is naturally oxidized. From Fig. 6(a) it is seen that the ZnO layer is thinner than the TiO$_2$ layer despite the fact that the nominal growth rate of 2 Å per cycle was expected for ZnO and 0.5 Å per cycle for TiO$_2$ which should have resulted in both layers having thicknesses of 40 nm. From the TEM images measured layer thicknesses of 35 nm for ZnO and 55–60 nm for TiO$_2$ were obtained. This observation suggests that there was a delay in the nucleation of the ZnO layer at the start of the ALD growth process. It is possible that ZnO may self-inhibit when growing on Si and as a result there may be a need to fine tune the recipe to correct this discrepancy.

In support of this proposal it is apparent that in contrast to the SiO$_2$/ZnO/TiO$_2$ structure, the SiO$_2$/TiO$_2$/ZnO structure shows similar layer thicknesses for the TiO$_2$ and ZnO layers, Fig. 6(b). From these TEM images it is evident that ZnO is crystalline due to clear lattice plane images being present in the TEM image and TiO$_2$ is amorphous which explains why no diffraction peaks were obtained in the XRD pattern on Si substrate.

Fig. 7 shows TEM images of true nanolaminate films. Again, the darker layers represent ZnO and the lighter coloured layers represent TiO$_2$. The nanolaminate remains intact and the layers
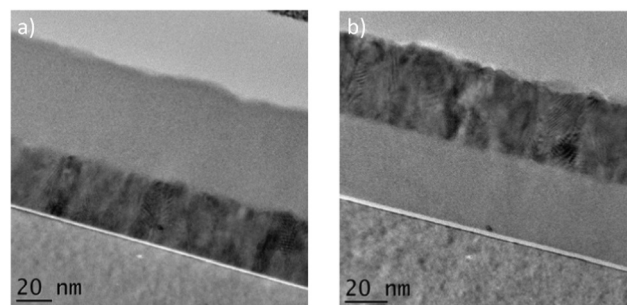


**Fig. 6** (a) TEM images of (a) the Si(100)/ZnO/TiO$_2$ and (b) the Si(100)/TiO$_2$/ZnO bilayer structures grown on the naturally-oxidized Si(100) substrates. Note the differences in layer thickness for the darker, ZnO layers when comparing both structures.
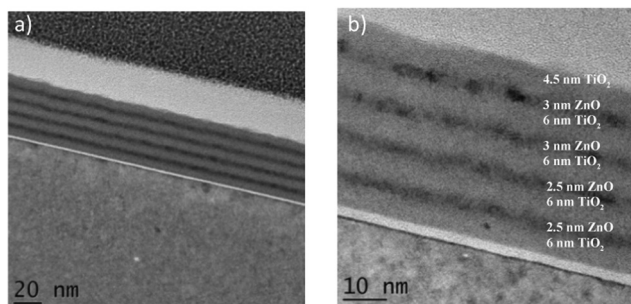
**Fig. 7** TEM images of ZnO and TiO$_2$ multilayers laminate (4 nm ZnO + 4 nm TiO$_2$) ×5 at (a) 20 nm and (b) 10 nm.

can clearly be distinguished. In support of the earlier proposal that the growth of the ZnO on the oxidized Si(100) surface is somewhat inhibited, from Fig. 7 it is possible to see clearly that the first of the very thin ZnO layers simply did not grow due to the proposed delay in nucleation. Interestingly in this example, the TiO$_2$ layers were thicker than expected, being some 6 nm as opposed to the expected 4 nm. The GPC of TiO$_2$ grown on ZnO appears to be greater than that of pure TiO$_2$ deposited directly on substrate. The opposite is observed with ZnO where the GPC of ZnO deposited on TiO$_2$ is reduced compared to that of pure ZnO grown directly on the substrate. This may be explained by considering surface chemisorption reactions. ALD is very sensitive to the chemical activity of the growth surface. Differences may exist in the chemical activity of the TDMAT and DEZn precursors and these differences could explain the resulting GPC values. A similar result has been observed in other ALD experiments.[57,58]

As seen in Fig. 8 the TEM images of the mixed ZnO/TiO$_2$ (1:1) layer reveal that after annealing some new deposits appear at the surface of the layer which also appears to have reduced in overall thickness from roughly 32 nm to 29 nm. Given the tendency of ZnO to readily form crystalline deposits it is proposed that the new deposits consisted on ZnO nanocrystals that form *via* segregation of Zn$^{2+}$ ions from the mixed layer, oxidation and crystallisation. With this proposal in mind ZnO lattice constants were calculated in accordance with Bragg's law[59] Using 1.54 Å for $\lambda$ (Cu K$\alpha$ radiation). The values for $d$; the interplanar spacing for ZnO(002) and (100) orientations are 2.68 Å and 2.9 Å respectively, confirming that the deposits were
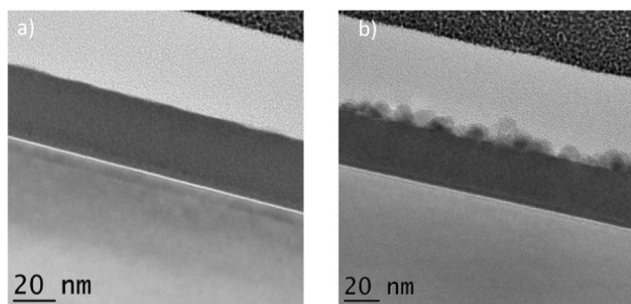


**Fig. 8** TEM images of the mixed 1:1 ZnO:TiO$_2$ (1:1) layer (a) before and (b) after, annealing at 400 °C for 60 minutes in air.
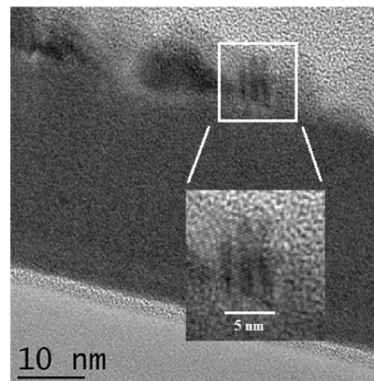


**Fig. 9** TEM image of the annealed mixed ZnO/TiO$_2$ layer focusing on one of the deposits that appear at the surface of the layer after annealing at 400 °C for 60 minutes in air.

most likely ZnO nanocrystals having a predominant orientation on the (002) direction as the interplanar spacing measurement was in agreement with the theoretical value. It has previously been reported that annealing ALD ZnO produces films preferentially oriented with the *c*-axis perpendicular to the substrate.[60,61] Fig. 9 shows the interplanar spacing within the ZnO nanocrystals as observed using TEM.

Atomic force microscopy (AFM) was employed to evaluate the surface topography of the ZnO, TiO$_2$ and ZnO/TiO$_2$ nanolaminate films. AFM images recorded for all films are presented in Fig. 10. The sampling surface area of the films analysed was $1 \times 1$ μm$^2$. The lighter coloured areas in the images indicate higher surface features. The $Z$ scale of the AFM data is situated to the left of each image. The $Z$ scale values vary from sample to sample with a maximum of $> 20$ nm for ZnO deposited on TiO$_2$ on glass substrate.

The RMS roughness was evaluated for each of the films. These results are displayed in Table 2. It can be seen from the results that RMS roughness increases for all films grown on glass substrates when compared to the same films deposited on Si substrate. This supports the proposal that growth is substrate-dependent as previously implied from the XRD results. Comparing TiO$_2$ and TiO$_2$ grown on ZnO, the RMS roughness values are practically the same on glass substrates, at *ca.* 1.49 nm and 1.5 nm respectively. However, the RMS roughness value doubles in the case of growth on the Si(100) substrate from 0.64 nm for TiO$_2$ alone to 1.2 nm for TiO$_2$ grown onto ZnO on Si(100). In other words the surface of the TiO$_2$ layer is considerably rougher when deposited onto ZnO grown on Si(100) as compared to that obtained when the TiO$_2$ was deposited directly on the Si(100) substrate.

Comparing ZnO and ZnO deposited onto TiO$_2$, again the RMS roughness values are very similar on glass substrates although a slight increase in RMS roughness is observed when the ZnO is deposited onto the TiO$_2$ layer grown on glass, having a slightly larger value at 1.77 nm as compared to 1.68 nm. Similarly the RMS roughness value obtained from the surface of the ZnO layer deposited onto the TiO$_2$ layer grown on the Si(100) substrate is again higher than that for ZnO grown
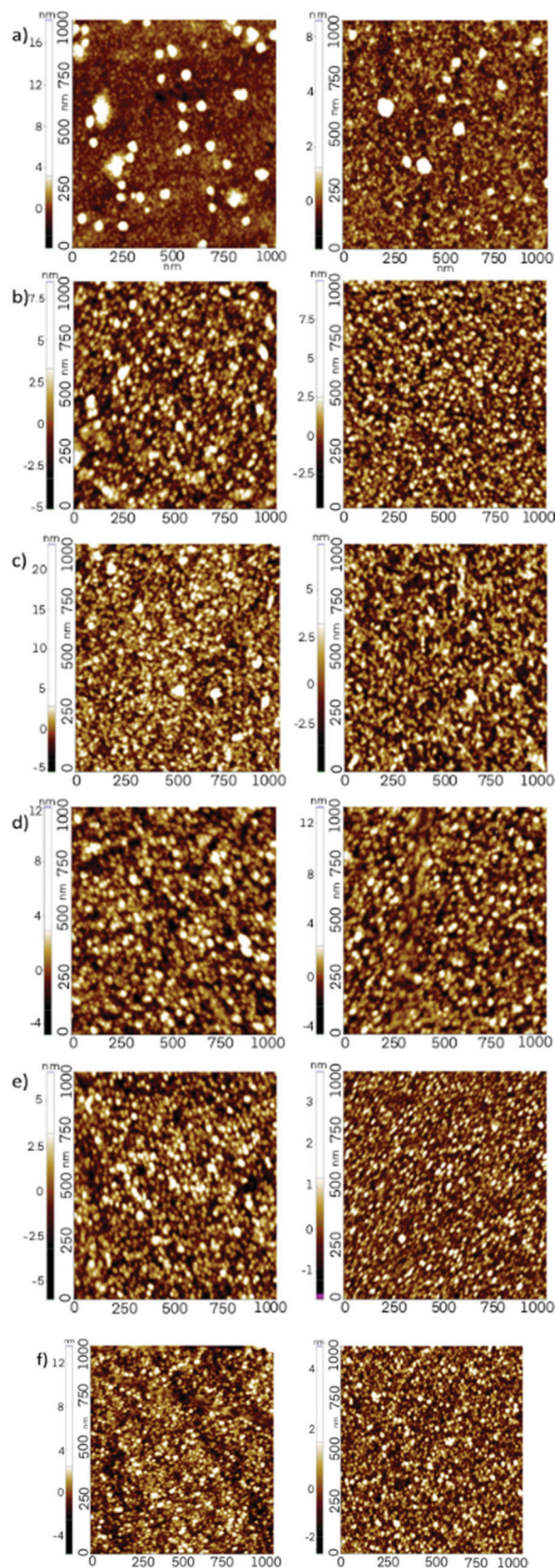
**Fig. 10** AFM images of (a) TiO$_2$, (b) ZnO, (c) ZnO on TiO$_2$, (d) TiO$_2$ on ZnO, (e) mixed ZnO : TiO$_2$ (1 : 1) layer and, (f) ×5 bilayers.

**Table 2** RMS roughness values for the various films produced here as a function of substrate type

| | RMS roughness of films grown on glass substrates (nm) | RMS roughness of films grown on Si(100) substrates (nm) |
|---|---|---|
| ZnO | 1.49 | 0.64 |
| TiO$_2$ | 1.68 | 1.27 |
| ZnO on TiO$_2$ | 1.77 | 1.64 |
| TiO$_2$ on ZnO | 1.50 | 1.21 |
| ZnO : TiO$_2$ (1 : 1) mixed layer | 1.63 | 0.61 |
| ZnO/TiO$_2$ ×5 | 1.24 | 0.80 |

directly on the Si(100) substrate, at 1.64 nm *versus* 1.27 nm, although the increase in RMS roughness isn't as substantial as that observed for the TiO$_2$ layer. For the nanolaminate stacks, RMS roughness values were found to be lower in comparison to the other films, being *ca.* 1.24 nm on glass and 0.8 nm on Si(100).

Interestingly, the mixed ZnO/TiO$_2$ 1 : 1 layer grown on a glass substrate had one of the highest results in terms of RMS roughness, at *ca.* 1.63 nm. In contrast, the same structure grown on the Si(100) substrate had one of the lowest RMS roughness values, at *ca.* 0.61 nm.

Fig. 10 below present AFM images for the nanolaminate films. For all images, films deposited on glass substrates are the left and films deposited on Si(100) substrates are on the right.

XPS was employed to characterise the chemical bonding and composition of the films. Fig. 11(a)–(c) show the XPS spectra of the Ti 2p, Zn 2p and O 1s peaks after mild argon-ion sputtering designed to remove the surface contamination that arises due to handling in air. The major doublet peaks at 459 eV and 465 eV in Fig. 11(a) can be assigned to Ti 2p$_{3/2}$ and Ti 2p$_{1/2}$ peaks of Ti–O bonding, consistent with the literature that exists for TiO$_2$.[48,62,63] The spectra can also be fitted with a second doublet at Ti 2p$_{3/2}$ at approx. 457.5 eV which can be attributed to Ti(III) oxide and hence Ti$^{3+}$.[62,63] The 2 peaks seen in Fig. 11(b) at 1021 eV and 1044 eV correspond to Zn 2p$_{3/2}$ and Zn 2p$_{1/2}$ and corresponds to accepted XPS data for ZnO found in the literature.[48] The O 1s spectrum depicted in Fig. 11(c) shows a peak at 529 eV which is attributed to oxygen bound to metal ions in the form of Ti–O and Zn–O species.[48]

The XPS data are entirely consistent with the growth of the target materials and do not indicate that layers are deficient in terms of any particular species. However, for the films which terminate in a TiO$_2$ layer, or for the deliberately mixed films, XPS can be particularly useful as a means of detecting Ti$^{3+}$ species which have been reported to play a crucial role in determining the photocatalytic activity of the film. Ti$^{3+}$ formation may arise from oxygen vacancies created as a result of oxygen diffusion.[64] Table 3 lists the percentage of Ti$^{3+}$ present in the TiO$_2$ only film, the ZnO/TiO$_2$ ×5 nanolaminate stack, the ZnO/TiO$_2$ bilayer nanolaminate and the ZnO : TiO$_2$ (1 : 1) as determined from the Ti 2p XPS data:

From Table 3 it may be seen that the layered nanolaminate structures has 20–25% of the titanium present as Ti$^{3+}$ and the
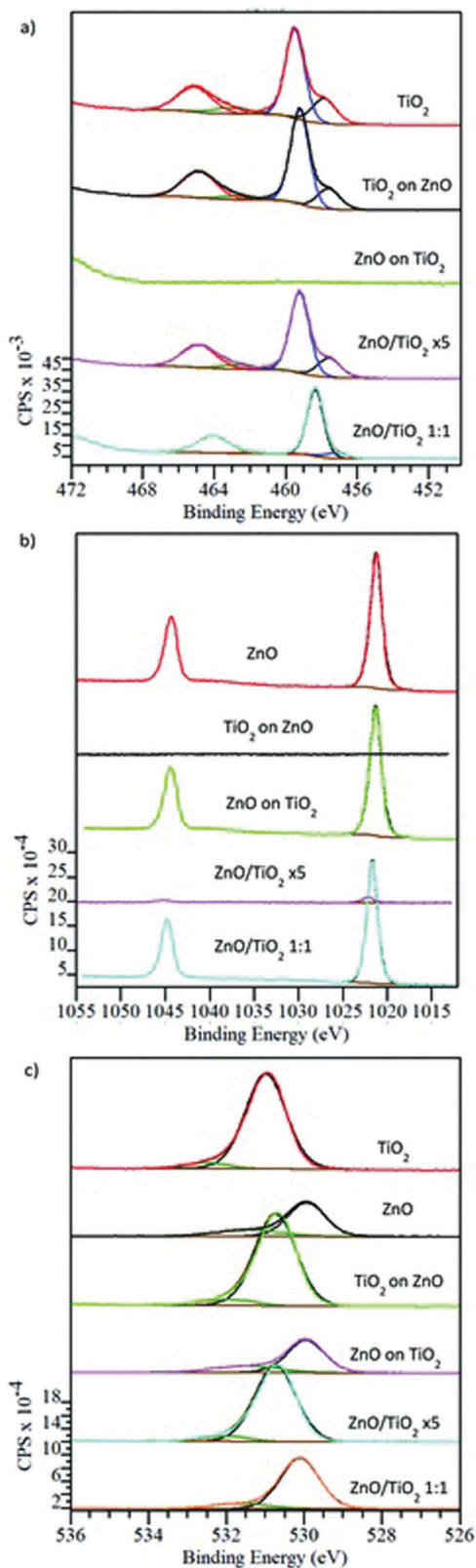
Fig. 11 XPS spectra on Si(100) substrates of (a) Ti 2p for $TiO_2$, $TiO_2$ on ZnO, ZnO on $TiO_2$, $ZnO/TiO_2$ ×5 and $ZnO:TiO_2$ (1:1) (b) Zn 2p for ZnO, $TiO_2$ on ZnO, ZnO on $TiO_2$, $ZnO/TiO_2$ ×5 and $ZnO:TiO_2$ (1:1) and (c) O 1s for $TiO_2$, ZnO $TiO_2$ on ZnO, ZnO on $TiO_2$, $ZnO/TiO_2$ ×5 and $ZnO:TiO_2$ (1:1).

Table 3   Percentages of $Ti^{3+}$ present in the various nanolaminate films studied

| Sample | % $Ti^{3+}$ |
| --- | --- |
| $TiO_2$ | 25.6 |
| $ZnO/TiO_2$ ×5 | 21.9 |
| $TiO_2$ on ZnO | 20.5 |
| $ZnO:TiO_2$ (1:1) | 8.8 |

rest as $Ti^{4+}$. These surfaces may provide photogenerated hole traps and assist with enhancing photocatalytic activity. Hole traps can increase the excited electron lifetimes located near the surface oxide species. This offers an opportunity for a greater chance of surface reactive oxide species (ROS) generation.[65–67] This will be further discussed in terms of photocatalytic activity later. However, mixed nanolaminate $ZnO:TiO_2$ (1:1) is seen to behave differently that it has a lower relative concentration of $Ti^{3+}$ and Ti $2p_{3/2}$ peak of the dominant Ti(IV) oxide is shifted to a lower binding energy of 458.3 eV suggesting that the immediate chemical/structural environment of the $Ti^{4+}$ is different to that of the other layered $TiO_2$ nanolaminates.

### Optical properties

The optical transmittance spectra for $ZnO:TiO_2$ (1:1), $ZnO/TiO_2$ (×5 bilayer), $ZnO/TiO_2$ and $TiO_2/ZnO$ bilayer nanolaminate structures grown on glass can be seen in Fig. 12. The average transmittance over the entirety of the visible wavelength range 400 to 550 nm is >60% rising to a maximum of ∼80% at 400 nm for the $TiO_2$ on ZnO sample and to ∼90% for the ZnO on $TiO_2$ sample. At 380 nm, a strong absorption peak is evident due to the fundamental band gaps of the materials. A slight bump is seen at 350 nm which may be a consequence of the film being a composite of two separate layers. The transmittance values for both films decline to ∼0% at lower wavelengths due to near complete absorption in the UV region. The $ZnO/TiO_2$ and $TiO_2/ZnO$ bilayer nanolaminates absorb more strongly in the UV/visible region in comparison to the
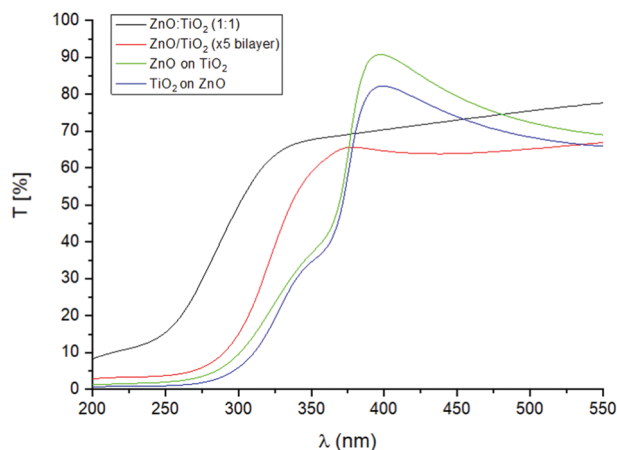


Fig. 12   Transmittance spectra of the $ZnO:TiO_2$ (1:1), $ZnO/TiO_2$ (×5 bilayer), $ZnO/TiO_2$ bilayer nanolaminate structures grown on glass.

$ZnO:TiO_2$ (1:1) and $ZnO/TiO_2$ (×5 bilayer) films. A blue shift in the wavelength of the absorption edge is observed with the $ZnO:TiO_2$ (1:1) and $ZnO/TiO_2$ (×5 bilayer) films with $ZnO:TiO_2$ (1:1) possessing the greatest effect on the shift. The blue shift observed may be explained by the Burstein–Moss effect. In this instance, the optical band gap of a semiconductor is increased with increasing electron concentration as the conduction band is occupied with excited electrons. The bottom of the conduction band is filled with donor electrons. According to Pauli's principle no two electrons may occupy the same state hence leading to a blockage in low-energy transitions which in turn enhances the optical band gap.[68] The structure of the latter films resemble that of Ti-doped ZnO (TZO). Hence, the carrier concentration may effectively be increased as Ti could be behaving as a donor material.

## Contact angle and photocatalytic activity

Contact angle (CA) measurements were taken in order to get an idea of the hydrophilic or hydrophobic nature of the films. In general a low surface energy and a rough microstructure equate to super-hydrophobicity.[69] The CA was measured prior to UV exposure, after 30 minutes and after 1 hour UV exposure. All values displayed are taken from films that had been annealed at 400 °C for 1 hour in air.

Initially, films grown on the glass substrates had lower CAs than those grown on Si(100) substrates. In some ways this would not be unexpected since XRD revealed that on these samples there was evidence of anatase formation and anatase is generally found to be the most photoactive form of $TiO_2$.[70] Following 30 minutes UV irradiation, the CAs decreased for all samples except for the $TiO_2$ on ZnO grown on glass sample (Fig. 13) and for $ZnO/TiO_2$ (×5 bilayers) grown on Si (Fig. 14). After 1 hour UV exposure, the CA for $TiO_2$ on ZnO grown on glass increased dramatically. Out of all the samples, the CAs for the $ZnO:TiO_2$ (1:1) films were found to be the some of the highest, however a slight decrease in CA with increasing irradiation time was observed. CAs of <5° were recorded for $TiO_2$ on glass after UV exposure which is indicative of super-hydrophilicity. This is again indicative of some photoactivity arising from the presence of some anatase. Although no general consensus exists to explain why, amorphous $TiO_2$ surfaces are not found to be particularly photoactive while anatase surfaces are the most photoactive.[70]

Morphological influences may also influence CA values. In our case particularly if the $TiO_2$ adopts the shape of the ZnO grown directly beneath it as in the case of the $TiO_2$ on ZnO grown on Si(100) substrate sample (see Fig. 4(c)). The CA data for this sample is shown in the red solid line in Fig. 13 and reveals that the CA remains high despite UV irradiation for an hour. In this particular case it would be tempting to assume that the very prominent texturing of the $TiO_2$ surface that arises from the ZnO template underneath dominates the CA response completely. However a similar level of texturing, albeit less uniform in nature, arises for $TiO_2$ on ZnO grown on a glass substrate and as may be seen from the red dotted line in Fig. 13 this material has a low CA value to start with which actually
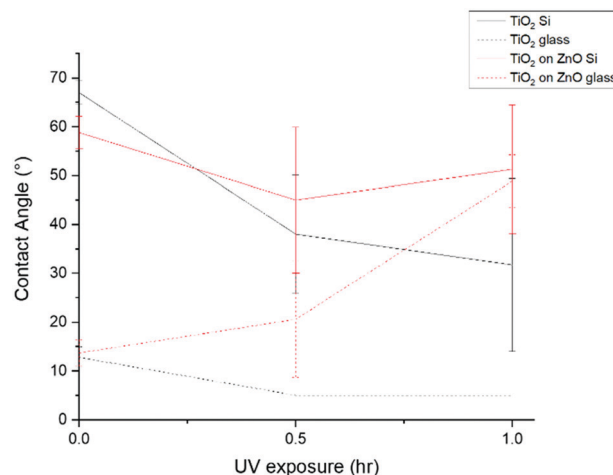


**Fig. 13** Contact angle measurements for $TiO_2$ and $TiO_2$ on ZnO grown on both Si(100) and glass substrates, after annealing at 400 °C for 1 hour in air and then exposed to UV radiation, as a function of time.



**Fig. 14** Contact angle measurements for $ZnO/TiO_2$ (×5 bilayers) and $ZnO:TiO_2$ (1:1) grown on both Si(100) and glass substrates, after annealing at 400 °C for 1 hour in air and then exposed to UV radiation, as a function of time.
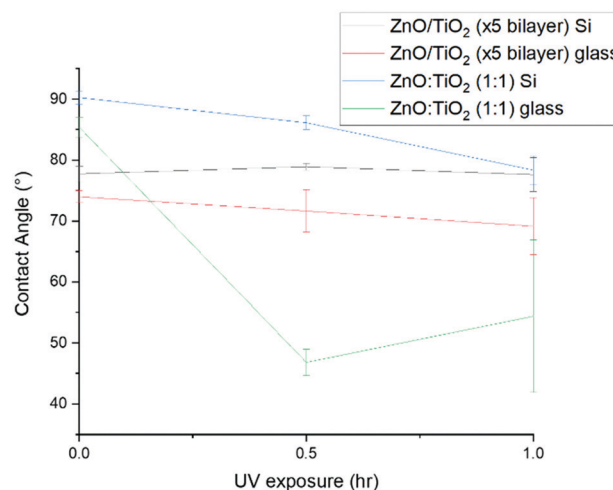
increases during UV exposure. Such potentially conflicting results are indicative of the fact that CA measurements are at best only a very rough guide to wards understanding the hydrophobicity or hydrophilicity of a sample surface.

Photocatalytic activity was also investigated *via* dye degradation experiments. Films were coated with an even layer of basic blue 66 dye and exposed to UV light and the change in the colour of the ink was monitored and recorded over time by use of a handheld digital scanner. Digital image analysis as described by Mills *et al.* was used to assess photo-activity of the films.[71]

Fig. 15 below shows the films initially covered with a thin layer of dye before UV exposure and after 150 minutes of UV bleaching.
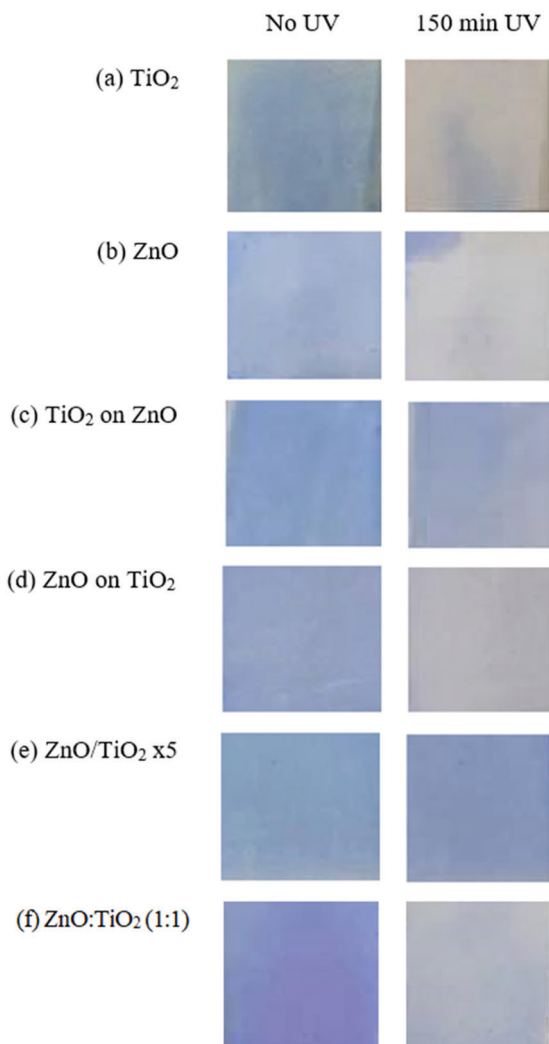
**Fig. 15** Images of the samples before and after 150 minutes UV irradiation on glass substrate: (a) $TiO_2$ (b) ZnO (c) $TiO_2$ on ZnO (d) ZnO on $TiO_2$ (e) ZnO/$TiO_2$ ×5 and (f) ZnO : $TiO_2$ (1 : 1).†

**Table 4** Times to bleach for $TiO_2$, ZnO, ZnO on $TiO_2$, $TiO_2$ on ZnO, ZnO/$TiO_2$ ×5 and ZnO : $TiO_2$ (1 : 1) films

| Sample | Time to bleach (minutes) |
|---|---|
| $TiO_2$ | 75.8 |
| ZnO | 69.3 |
| ZnO on $TiO_2$[a] | 116.4 |
| $TiO_2$ on ZnO | 130.8 |
| ZnO/$TiO_2$ ×5 | — |
| ZnO : $TiO_2$ (1 : 1)[b] | 77.2 |

[a] Two separate films of ZnO on $TiO_2$ were analysed so the average of both values is being used for time to bleach. [b] Sample has been annealed at 400 °C for 60 minutes in air.

Although some of the films display some degree of photo-activity, the shortest time-to-bleach as determined by visual inspection was around 69 minutes exposure.

By assessment of the time-to-bleach values given in Table 4, it may be seen that the ZnO and $TiO_2$ films are the most photoactive, followed closely by ZnO : $TiO_2$ (1 : 1). A value for the time to bleach ZnO/$TiO_2$ ×5 bilayer could not be calculated.

The results from the dye degradation experiments are in good agreement with the CA values obtained for the films after 1 hour UV exposure. Interestingly, XPS results revealed that the $TiO_2$ on ZnO film contained the highest percentage of $Ti^{3+}$ on its surface. However, CA and dye degradation experiments suggest that this film is not particularly photoactive. The presence of $Ti^{3+}$ influences the electronic structure and surface activity of $TiO_2$.[72] In particular it is likely that the presence of $Ti^{3+}$ extends the wavelength range where the material absorbs into the visible region of the spectrum. If this were the case then it might provide a mechanism whereby the visible light-induced photocatalytic activity could become significant.[73–77] However as noted above, these samples were not found to be photoactive using the tests employed.

By comparing the before and after images presented in Fig. 15, it is concluded that the dye did not degrade to any visual degree on the ZnO/$TiO_2$ ×5 nanolaminate stack grown on glass suggesting nearly complete inactivity (samples (e) in Fig. 15). For the samples shown in (c) in these figures which were the ZnO/$TiO_2$ bilayer samples grown on glass with the $TiO_2$ layer on top of the ZnO layer, the dye only showed slight discolouration suggesting that this sample had some, albeit minimal levels of photoactivity.

Comparing the samples shown in (c) $TiO_2$ on ZnO and (d) ZnO on $TiO_2$ (c) in these figures, the dye was again degraded suggesting that these films also possessed some degree of photoactivity. Similarly the samples shown in (f) also degraded the dye to some extent showing photoactivity.

## Conclusions

$TiO_2$/ZnO nanolaminates were deposited *via* an ALD process which revealed a slight delay in nucleation with ZnO. SEM showed that $TiO_2$ morphology follows that of the ZnO underneath. XRD results suggested that layer growth was substrate-dependent as crystalline $TiO_2$ was only identified on glass. The ZnO was polycrystalline as evidenced by the appearance lattice fringes in the TEM images while the $TiO_2$ was amorphous. TEM revealed that the laminates remained intact after annealing. Nanocrystals were seen on top of the mixed Zn : Ti (1 : 1) film and thus it is apparent that the mixed film is not stable towards high temperature annealing. These results suggest that formation of a nanolaminate structure may help with stability. After 1 hour UV exposure, the $TiO_2$ yielded a CA value of $<5°$, suggesting superhydrophilicity.

This study highlights how the use of an underlayer may act as a template of morphology. It also suggests the possible role of nanolaminates in stabilizing materials. In a practical sense, $TiO_2$ may act as a stabilizer for ZnO in a $TiO_2$/ZnO bilayer stack

† Sample has been annealed at 400 °C for 60 minutes in air.

when used as an anode material in lithium ion batteries (LIBs).[78]

## Author contributions

S. D. fabricated nanolaminate films, carried out; SEM analysis (supervised by Vincent Lodge at Tyndall National Institute), optical measurements, contact angle measurements and photocatalytic activity experiments (supervised by Harry Manley at Tyndall National Institute). S. D. also prepared the manuscript. L. R. and M. M. M. fabricated nanolaminate films. M. M. carried out GIXRD and AFM analysis. M. S. carried out FIB/TEM analysis. F. L. carried out the XPS analysis. All authors have given approval to the final version of the manuscript.

## Conflicts of interest

There are no conflicts to declare.

## Acknowledgements

## Notes and references

1 B. Radisavljevic, A. Radenovic, J. Brivio, V. Giacometti and A. Kis, Single-layer $MoS_2$ transistors, *Nat. Nanotechnol.*, 2011, **6**(3), 147–150.

2 O. Lopez-Sanchez, D. Lembke, M. Kayci, A. Radenovic and A. Kis, Ultrasensitive photodetectors based on monolayer $MoS_2$, *Nat. Nanotechnol.*, 2013, **8**(7), 497–501.

3 S. Bertolazzi, J. Brivio and A. Kis, Stretching and Breaking of Ultrathin $MoS_2$, *ACS Nano*, 2011, **5**(12), 9703–9709.

4 H. Zeng, J. Dai, W. Yao, D. Xiao and X. Cui, Valley polarization in MoS2 monolayers by optical pumping, *Nat. Nanotechnol.*, 2012, **7**, 490–493.

5 W. Zhang, C. P. Chuu, J. K. Huang, C. H. Chen, M. L. Tsai, Y. H. Chang, C. T. Liang, Y. Z. Chen, Y. L. Chueh, J. H. He, M. Y. Chou and L. J. Li, Ultrahigh-Gain Photodetectors Based on Atomically Thin Graphene-$MoS_2$ Heterostructures, *Sci. Rep.*, 2014, **23**(4), 3826.

6 C. Cong, J. Shang, X. Wu, B. Cao, N. Peimyoo, C. Qiu, L. Sun and T. Yu, Synthesis and Optical Properties of Large-Area Single-Crystalline 2D Semiconductor $WS_2$ Monolayer from Chemical Vapor Deposition, *Adv. Opt. Mater.*, 2014, **2**, 131–136.

7 Y. Cai, J. Lan, G. Zhang and Y. W. Zhang, Lattice vibrational modes and phonon thermal conductivity of monolayer $MoS_2$, *Phys. Rev. B: Condens. Matter Mater. Phys.*, 2014, **89**, 035438.

8 J. Azadmanjiri, C. C. Berndt, J. Wang, A. J. Kapoor and V. K. Srivastavac, Nanolaminated composite materials: structure, interface role and applications, *RSC Adv.*, 2016, **6**, 109361.

9 P. Sundberg and M. Karppinen, Organic and inorganic-organic thin film structures by molecular layer deposition: a review, *Beilstein J. Nanotechnol.*, 2014, **5**, 1104–1136.

10 D. F. Schmidt, Nanolaminates - Bioinspired and beyond, *Mater. Lett.*, 2013, **108**, 328–335.

11 J. Azadmanjiri, C. C. Berndt, J. Wang, A. J. Kapoor, V. K. Srivastavac and C. Wen, A review on hybrid nanolaminate materials synthesized by deposition techniques for energy storage applications, *J. Mater. Chem. A*, 2014, **2**, 3695–3708.

12 M. Puttaswamy, M. Vehkamäki, K. Kukli, M. C. Dimri, M. Kemmel, T. Hatanpää, M. J. Heikkilä, K. Mizohata, R. Stern, M. Ritala and M. Leskelä, Bismuth iron oxide thin films using atomic layer deposition of alternating bismuth oxide and iron oxide layers, *Thin Solid Films*, 2016, **611**, 78–87.

13 G. Zhang, H. Wu, X. Wang, D. Zhang, T. Wang and C. Liu, Modulation of the dissipation factor in transparent AlZnO/$ZrO_2$/AlZnO capacitors, *J. Alloys Compd.*, 2017, **690**, 777–782.

14 J. R. Martínez-Castelo, J. López, D. Domínguez, E. Murillo, R. Machorro, H. A. Borbón-Nuñez, I. Fernandez-Alvarez, A. Arias, M. Curiel, N. Nedev, M. H. Farías and H. Tiznado, Structural and electrical characterization of multilayer $Al_2O_3$/ZnO nanolaminates grown by atomic layer deposition, *Mater. Sci. Semicond. Process.*, 2017, **71**, 290–295.

15 T. Onaya, T. Nabatame, T. Sawada, K. Kurishima, N. Sawamoto, A. Ohi and A. Ogura, Improved leakage current properties of $ZrO_2$/(Ta/Nb)O$_x$ -$Al_2O_3$/$ZrO_2$ nanolaminate insulating stacks for dynamic random access memory capacitors, *Thin Solid Films*, 2018, **655**, 48–53.

16 W. Chen, W. Ren, Y. Zhang, M. Liu and Z. G. Ye, Preparation and properties of $ZrO_2$ and $TiO_2$ films and their nanolaminates by atomic layer deposition, *Ceram. Int.*, 2015, **41**, S278–S282.

17 A. Rodríguez, M. B. Gonzalez, F. Campabadal, J. Suñé and E. Miranda, Electrical characterization of multiple leakage current paths in $HfO_2$/$Al_2O_3$-based nanolaminates, *Microelectron. Reliab.*, 2015, **55**(9-10), 1442–1445.

18 H. Cho, K. W. Park, C. H. Park, H. J. Cho, S. J. Yeom, K. Hong, N. J. Kwak and J. H. Ahn, Abnormally enhanced dielectric constant in $ZrO_2$/$Ta_2O_5$ multi-laminate structures by metallic Ta formation, *Mater. Lett.*, 2015, **154**, 148–151.

19 J. López, J. Martínez, N. Abundiz, D. Domínguez, E. Murillo, F. Castillón, R. Machorro, M. Farías and H. Tiznado, Thickness effect on the optical and morphological properties in $Al_2O_3$/ZnO nanolaminate thin films prepared by atomic layer deposition, *Superlattices Microstruct.*, 2016, **90**, 265–273.

20 R. Lo Nigro, E. Schilirò, G. Greco, P. Fiorenza and F. Roccaforte, Laminated $Al_2O_3$–$HfO_2$ layers grown by atomic layer deposition for microelectronics applications, *Thin Solid Films*, 2016, **601**, 68–72.

21 C. Mahata, Y. An, S. Choi, Y. C. Byun, D. K. Kim, T. Lee, J. Kim, M. H. Cho and H. Kim, Electrical properties of the HfO$_2$–Al$_2$O$_3$ nanolaminates with homogeneous and graded compositions on InP, *Curr. Appl. Phys.*, 2016, **16**(3), 294–299.

22 J. Zhang, X. Ding, J. Li, H. Zhang, X. Jiang and Z. Zhang, Performance enhancement in InZnO thin-film transistors with compounded ZrO$_2$–Al$_2$O$_3$ nanolaminate as gate insulators, *Ceram. Int.*, 2016, **42**(7), 8115–8119.

23 J. Gao, G. He, Z. Sun, H. Chen, C. Zheng, P. Jin, D. Xiao and M. Liu, Modification of electrical properties and carrier transportation mechanism of ALD-derived HfO$_2$/Si gate stacks by Al$_2$O$_3$ incorporation, *J. Alloys Compd.*, 2016, **667**, 352–358.

24 A. Rodriguez, M. B. Gonzalez, F. Campabadal, J. Suñé and E. Miranda, Breakdown time statistics of successive failure events in constant voltage-stressed Al$_2$O$_3$/HfO$_2$ nanolaminates, *Microelectron. Eng.*, 2015, **147**, 85–88.

25 C. Mahata, Y. C. Byun, C. H. An, S. Choi, Y. An and H. Kim, Comparative study of atomic-layer-deposited stacked (HfO2/Al2O3) and nanolaminated (HfAlOx) dielectrics on In$_{0.53}$Ga$_{0.47}$As, *ACS Appl. Mater. Interfaces*, 2013, **5**(10), 4195–4201.

26 L. H. Kim, K. Kim, S. Park, Y. J. Jeong, H. Kim, D. S. Chung, S. H. Kim and C. E. Park, Al$_2$O$_3$/TiO$_2$ Nanolaminate Thin Film Encapsulation for Organic Thin Film Transistors via Plasma-Enhanced Atomic Layer Deposition, *ACS Appl. Mater. Interfaces*, 2014, **6**, 6731–6738.

27 A. Singh, F. Nehm, L. Müller-Meskamp, C. Hoßbach, M. Albert, U. Schroeder, K. Leo and T. Mikolajick, OLED compatible water-based nanolaminate encapsulation systems using ozone based starting layer, *Org. Electron.*, 2014, **15**, 2587–2592.

28 J. Oh, S. Shin, J. Park, G. Ham and H. Jeon, Characteristics of Al$_2$O$_3$/ZrO$_2$ laminated films deposited by ozone-based atomic layer deposition for organic device encapsulation, *Thin Solid Films*, 2016, **599**, 119–124.

29 E. G. Jeong, Y. C. Han, H. G. Im, B. S. Bae and K. C. Choi, Highly reliable hybrid nano-stratified moisture barrier for encapsulating flexible OLEDs, *Org. Electron.*, 2016, **33**, 150–155.

30 F. Nehm, F. Dollinger, H. Klumbies, L. Müller-Meskamp, K. Leo, A. Singh, C. Richter, U. Schroeder, T. Mikolajick, C. Hossbach, M. Albert and J. W. Bartha, Atomic layer deposited TiO$_x$/AlO$_x$ nanolaminates as moisture barriers for organic devices, *Org. Electron.*, 2016, **38**, 84–88.

31 J. Leppäniemi, P. Sippola, M. Broas, J. Aromaa, H. Lipsanen and J. Koskinen, Corrosion protection of steel with multi-layer coatings: Improving the sealing properties of physical vapor deposition CrN coatings with Al$_2$O$_3$/TiO$_2$ atomic layer deposition nanolaminates, *Thin Solid Films*, 2017, **627**, 59–68.

32 P. A. Radi, G. E. Testoni, R. S. Pessoa, H. S. Maciel, L. A. Rocha and L. Vieira, Tribocorrosion behavior of TiO$_2$/Al$_2$O$_3$ nanolaminate, Al$_2$O$_3$, and TiO$_2$ thin films produced by atomic layer deposition, *Surf. Coat. Technol.*, 2018, **349**, 1077–1082.

33 B. Díaz, E. Härkönen, J. Świątowska, A. Seyeux, V. Maurice, M. Ritala and P. Marcus, Corrosion properties of steel protected by nanometre-thick oxide coatings, *Corros. Sci.*, 2014, **82**, 208–217.

34 E. Härkönen, S. Tervakangas, J. Kolehmainen, B. Díaz, J. Swiatowska, V. Maurice, A. Seyeux, P. Marcus, M. Fenker, L. Tóth, G. Radnóczi and M. Ritala, Interface control of atomic layer deposited oxide coatings by filtered cathodic arc deposited sublayers for improved corrosion protection, *Mater. Chem. Phys.*, 2014, **147**, 895–907.

35 H. Mohseni and T. W. Scharg, Role of atomic layer deposited solid lubricants in the sliding wear reduction of carbon–carbon composites at room and higher temperatures, *Wear*, 2015, **332-333**, 1303–1313.

36 J. López, H. A. Borbón-Nuñez, E. G. Lizarraga-Medina, E. Murillo, R. Machorro, N. Nedev and G. Soto, Al2O3-Y2O3 ultrathin multilayer stacks grown by atomic layer deposition as perspective for optical waveguides applications, *Opt. Mater.*, 2017, **72**, 788–794.

37 N. Pinna and M. Knez, *Atomic Layer Deposition of Nanostructured Materials*, Wiley-VCH: Weinheim, Germany, 2012.

38 H. B. Lee, V. R. Anderson and S. M. George, Growth and Properties of Hafnicone and HfO$_2$/Hafnicone Nanolaminates and Alloy Films Using Molecular Layer Deposition Techniques, *ACS Appl. Mater. Interfaces*, 2014, **6**, 16880–16887.

39 M. Leskelä and M. Ritala, Atomic layer deposition (ALD): from precursors to thin film structures, *Thin Solid Films*, 2002, **409**, 138–146.

40 R. W. Johnson, A. Hultqvist and S. F. Bent, A brief review of atomic layer deposition: from fundamentals to applications, *Mater. Today*, 2014, **17**(5), 236–246.

41 C. A. P. Handwerker and T. M. Pollock, Emerging Science and Research Opportunities for Metals and Metallic Nanostructures, *JOM*, 2014, **66**(7), 1321–1341.

42 A. Janotti and C. G. Van de Walle, Fundamentals of zinc oxide as a semiconductor, *Rep. Prog. Phys.*, 2009, **72**, 126501.

43 D. Reyes-Coronado, G. Rodríguez-Gattorno, M. E. Espinosa-Pesqueira, C. Cab, R. de Coss and G. Oskam, Phase-pure TiO$_2$ nanoparticles: anatase, brookite and rutile, *Nanotechnology*, 2008, **19**, 145605.

44 L. Xu, L. Shi and X. Li, Effect of TiO$_2$ buffer layer on the structural and optical properties of ZnO thin films deposited by E-beam evaporation and sol-gel method, *Appl. Surf. Sci.*, 2008, **255**, 3230–3234.

45 J. Tian, L. Chen, Y. Yin, X. Wang, J. Dai, Z. Zhu, X. Liu and P. Wu, Photocatalyst of TiO$_2$/ZnO nano composite film: Preparation, characterization, and photodegradation activity of methyl orange, *Surf. Coat. Technol.*, 2009, **204**, 205–214.

46 P. Prasannalakshmi and N. Shanmugam, Fabrication of TiO$_2$/ZnO nanocomposites for solar energy driven photocatalysis, *Mater. Sci. Semicond. Process.*, 2017, **61**, 114–124.

47 Y. Z. Gu, H. L. Lu, Y. Geng, Z. Y. Ye, Y. Zhang, Q. Q. Sun, S. J. Ding and D. W. Zhang, Optical and microstructural properties of ZnO/TiO$_2$ nanolaminates, *Nanoscale Res. Lett.*, 2013, **8**, 107.

48  X. Qian, M. Y. Gao, Y. Q. Cao, B. L. Guo and A. D. Li, Preparation and phase structures of Zn–Ti–O ternary compounds by atomic layer deposition, *J. Vac. Sci. Technol., A*, 2013, **31**.

49  W. K. Wang, H. C. Wen, C. H. Cheng, C. H. Hung, W. C. Chou, W. H. Yau, P. F. Yang and Y. S. Lai, Nanotribological properties of ALD-processed bilayer TiO$_2$/ZnO films, *Microelectron. Reliab.*, 2014, **54**, 2754–2759.

50  R. Chen, J. L. Lin, W. J. He, C. L. Duan, Q. Peng and X. L. Wang, Spatial atomic layer deposition of ZnO/TiO$_2$ nanolaminates, *J. Vac. Sci. Technol., A*, 2016, **34**, 5.

51  A. Leelavathi, G. Madras and N. Ravishankar, Origin of enhanced photocatalytic activity and photoconduction in high aspect ratio ZnO nanorods, *Phys. Chem. Chem. Phys.*, 2013, **15**, 10795–10802.

52  C. Han, M.-Q. Yang, B. Weng and Y.-J. Xu, Improving the photocatalytic activity and anti-photocorrosion of semiconductor ZnO by coupling with versatile carbon, *Phys. Chem. Chem. Phys.*, 2014, **16**, 16891–16903.

53  W. Li, G. Wang, C. Chen, J. Liao and Z. Li, Enhanced Visible Light Photocatalytic Activity of ZnO Nanowires Doped with Mn$^{2+}$ and Co$^{2+}$ Ions, *Nanomaterials*, 2017, **7**(1), 20.

54  E. Rokhsat and O. Akhavan, Improving the photocatalytic activity of graphene oxide/ZnO nanorod films by UV irradiation, *Appl. Surf. Sci.*, 2016, **371**, 590–595.

55  P. Scherrer, Bestimmung der Größe und der inneren Struktur von Kolloidteilchen mittels Röntgenstrahlen, *Nachr. Ges. Wiss. Goettingen, Math.-Phys. Kl.*, 1918, 98.

56  H. Abrams, Grain Size Measurement by the Intercept Method, *Metallography*, 1971, **4**(1), 59–78.

57  P. Poodt, A. Lankhorst, F. Roozeboom, K. Spee, D. Maas and A. Vermeer, High-Speed Spatial Atomic-Layer Deposition of Aluminum Oxide Layers for Solar Cell Passivation, *Adv. Mater.*, 2010, **22**(32), 3564–3567.

58  M. Vehkamäki, T. Hatanpää, M. Ritala and M. Leskelä, Bismuth precursors for atomic layer deposition of bismuth-containing oxide films, *J. Mater. Chem.*, 2004, **14**(21), 3191–3197.

59  W. H. Bragg, The Reflection of X-rays by Crystals, *Proc. R. Soc. London, Ser. A*, 1913, **88**(605), 428–438.

60  J.-L. Tian, H.-Y. Zhang, G.-G. Wang, X.-Z. Wang, R. Sun, L. Jin and J.-C. Han, Influence of film thickness and annealing temperature on the structural and optical properties of ZnO thin films on Si(100) substrates grown by atomic layer deposition, *Superlattices Microstruct.*, 2015, **83**, 719–729.

61  C.-Y. Yen, S.-R. Jian, G.-J. Chen, C.-M. Lin, H.-Y. Lee, W.-C. Ke and J.-Y. Juang, Influence of annealing temperature on the structural, optical and mechanical properties of ALD-derived ZnO thin films, *Appl. Surf. Sci.*, 2011, **257**(17), 7900–7905.

62  B. Bharti, S. Kumar, H. N. Lee and R. Kumar, Formation of oxygen vacancies and Ti3+ state in TiO2 thin film and enhanced optical properties by air plasma treatment, *Sci. Rep.*, 2016, **6**, 1–13.

63  P. Chen, A novel synthesis of Ti$^{3+}$ self-doped Ag$_2$O/TiO$_2$ (p-n) nanoheterojunctions for enhanced visible photocatalytic activity, *Mater. Lett.*, 2016, **163**, 130–133.

64  Y. Zhang, Z. P. Xing, X. F. Liu, Z. Z. Li, X. Y. Wu, J. J. Jiang, M. Li, Q. Zhu and W. Zhou, Ti3+ self-doped blue TiO2 single-crystalline nanorods for efficient solar driven photocatalytic performance, *ACS Appl. Mater. Interfaces*, 2016, **8**(40), 26851–26859.

65  A. L. Linsebigler, G. Q. Lu and J. T. Yates, Photocatalysis on TiO2 surfaces - Principles, mechanisms and selected results, *ACS Appl. Mater. Interfaces*, 1995, **8**(40), 26851–26859.

66  M. Muruganandham and M. Swaminathan, Solar photocatalytic degradation of a reactive azo dye in TiO$_2$-suspension, *Sol. Energy Mater. Sol. Cells*, 2004, **81**(4), 439–457.

67  M. A. Fox and M. T. Dulay, Heterogeneous photocatalysis, *Chem. Rev.*, 1993, **93**(1), 341–357.

68  F. K. Shan, G. X. Liu, W. J. Lee and B. C. Shin, Stokes shift, blue shift and red shift of ZnO-based thin films deposited by pulsed-laser deposition, *J. Cryst. Growth*, 2006, **291**, 328–333.

69  M. Nosonovsky and B. Bhushan, in *Multiscale Dissipative Mechanisms and Hierarchical Surfaces*, Springer, Berlin, Heidelberg, 1st edn, 2008, ch. 6, pp. 81–113.

70  T. Luttrell, S. Halpegamage, J. Tao, A. Kramer, E. Sutter and M. Batzill, Why is anatase a better photocatalyst than rutile? - Model studies on epitaxial TiO$_2$ films, *Sci. Rep.*, 2015, **4**, 4043.

71  A. Mills, C. O'Rourke and N. Wells, A smart ink for the assessment of low activity photocatalytic surfaces, *Analyst*, 2014, **139**, 5409.

72  Y. Xu, S. Wu, P. Wan, J. Sun and Z. D. Hood, Introducing Ti$^{3+}$ defects based on lattice distortion for enhanced visible light photoreactivity in TiO2 microspheres, *RSC Adv.*, 2017, **7**, 32461.

73  L. R. Grabstanowicz, S. Gao and T. Li, *et al.*, Facile Oxidative Conversion of TiH$_2$ to High-Concentration Ti$^{3+}$ - Self-Doped Rutile TiO$_2$ with Visible-Light Photoactivity, *Inorg. Chem.*, 2013, **52**, 3884–3890.

74  X. Chen, L. Liu and F. Huang, Black Titanium Dioxide (TiO$_2$) Nanomaterials, *Chem. Soc. Rev.*, 2015, **44**, 1861–1885.

75  P. Deak, B. Aradi and T. Frauenheim, Oxygen deficiency in TiO$_2$: Similarities and differences between the Ti self-interstitial and the O vacancy in bulk rutile and anatase, *Phys. Rev. B: Condens. Matter Mater. Phys.*, 2015, **92**(4), 045204.

76  L. Aïnouche, L. Hamadou, A. Kadri, N. Benbrahim and D. Bradai, Ti$^{3+}$ states induced band gap reduction and enhanced visible light absorption of TiO$_2$ nanotube arrays: Effect of the surface solid fraction factor, *Sol. Energy Mater. Sol. Cells*, 2016, **151**, 179–190.

77  X. Lui, G. Du and M. Li, True Photoreactivity Origin of Ti$^{3+}$ - Anatase TiO$_2$ crystals with Respectively Dominated Exposed {001}, {101}, and {100} Facets, *ACS Omega*, 2019, **4**, 14902–14912.

78  Y. Q. Cao, S.-S. Wang, C. Liu, D. Wu and A.-D. Li, Atomic layer deposition of ZnO/TiO$_2$ nanolaminates as ultra-long life anode material for lithium-ion batteries, *Sci. Rep.*, 2019, **9**, 11526.